Impact of Gas Composition on Natural Gas Storage by Adsorption

José P. B. Mota
Dept. de Química, Centro de Química Fina e Biotecnologia, Universidade Nova de Lisboa, 2825-114 Caparica, Portugal

Adsorption storage is the most promising low-pressure alternative for storing natural gas, but some operational difficulties hinder the success of this technology. From a modeling perspective, this article addresses the impact of gas composition on the cyclic behavior of adsorptive natural gas storage systems. The cyclic operation of an onboard storage reservoir is modeled as a series of consecutive two-step processes, each consisting of charge with a fixed composition gas mixture followed by discharge at constant molar flow rate. Special attention is given to the composition and calorific value of the gas delivered by the storage system and to performance quantifiers that measure net deliverable capacity as a function of cycle number. Evidence of a cyclic steady state is given, and the numerical results are compared with experimental measurements. The results show the need for identifying and evaluating economical means of removing the higher molecular-weight hydrocarbons and other highly adsorbed species from the gas stream before charging the storage reservoir.

Introduction

Natural gas (NG) has always been considered a potentially attractive fuel for vehicle use. It is cheaper than gasoline and diesel, the technical feasibility of NG vehicles (NGVs) is well established, and these vehicles have a less adverse effect on the environment than liquid-fueled vehicles. For example, NG can be burned in such a way as to easily minimize NO_x and CO emissions (Parkyns and Quinn, 1995).

NG is about 95% methane, a gas that cannot be liquefied at ambient temperature ($T_c = -82.6$°C). Since it is a gaseous fuel, its volumetric energy content is low compared with those of liquid fuels. In fact, NG outscores petroleum-based fuels in every aspect except onboard storage (Talu, 1992). Currently, NG is compressed at pressures up to 25 MPa in order to be stored compactly on-board and dispensed quickly. This storage method requires expensive and heavy high-pressure compression technology, which has been the major economic bottleneck for the wide acceptance of NG as a transportation fuel (Remick et al., 1984).

A large effort has been invested in the replacement of high-pressure compression by an alternative storage method working at pressures up to 3.5 MPa. Besides allowing the use of lighter and safer onboard storage reservoirs, this upper pressure limit can be easily achieved with a single-stage compressor or, alternatively, the vehicle can be refueled directly from a high-pressure NG pipeline. This way, a significant decrease in the capital and operating costs of compression stations is achieved.

Adsorption storage is regarded now as the most promising low-pressure alternative for storing NG. Most research on adsorbed natural gas (ANG) storage has aimed at the development and evaluation of adsorbents with storage capacities comparable to that of compressed NG. Microporous activated carbon with high packing density has emerged as the best adsorbent for ANG storage. Reviews surveying the recent developments in this area were published by Parkyns and Quinn (1995) and Talu (1992); an update of the former review will be published shortly (Cook et al., 1999).

Several operational problems that hinder the success of ANG technology have been addressed in the literature. The one of concern in this work is the adsorbent-capacity deterioration on extended operation due to the nature of NG composition. Besides methane, NG contains ethane, nitrogen, and a small proportion of alkanes ranging from C_3 to C_7. Carbon dioxide may also be present in small quantities (0.04 to 1% molar), as well as water vapor in the concentration range 75–180 ppm (v/v), and sulfur-containing compounds at the ppm level (Parkyns and Quinn, 1995).

These species, mainly the higher molecular-weight hydrocarbons, are more strongly adsorbed than methane, especially in the low-pressure region. This behavior is depicted in

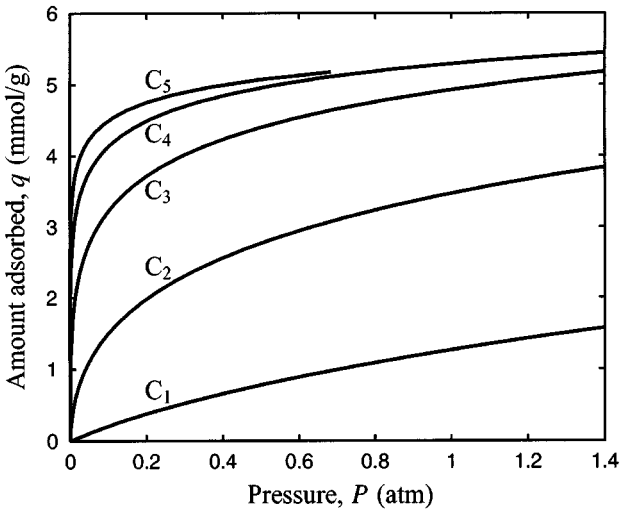

Figure 1. Single-component isotherms for hydrocarbon adsorption on activated carbon at 25°C.

The isotherms for C_2–C_5 were calculated by applying the Adsorption Potential theory to the experimental methane data, based on the procedure described in this article. C_1: methane; C_2: ethane; C_3: propane; C_4: butane; C_5: pentane.

Figure 1 that shows the single-component adsorption isotherms at room temperature for the first five alkanes on activated carbon. If the higher molecular-weight hydrocarbons are allowed to enter the onboard storage system during charge, they adsorb preferentially and decrease the amount of gas that can actually be deliverable by the storage system. This is driven by the unfeasibility of operating an onboard storage reservoir under subatmospheric pressure, since excessive compression hardware would be necessary to extract and boost the fuel pressure (Talu, 1992).

The depletion pressure considered in this work is 1.4 atm, and it is the same as the upper pressure value employed in Figure 1. For this pressure, Table 1 lists the values of limiting selectivity and isotherm slope ratio for the adsorption of alkanes C_2–C_5 on the same activated carbon of Figure 1. The limiting selectivity, $s^0_{i,1}$, is the selectivity of species i in a binary mixture consisting essentially of methane. It takes into account the nature of NG composition, although it neglects the interaction between the other hydrocarbons. Table 1 shows that $s^0_{i,1}$ increases drastically and that the isotherm flattens with increasing hydrocarbon molecular weight. Thus, the ''impurities'' are not preferentially desorbed during discharge and they tend to accumulate in the storage tank on cyclic operation. This undesirable phenomenon has been observed experimentally by some researchers (Czepirski, 1991; Golovoy and Blais, 1983; Kasuh et al., 1992; Parkyns and Quinn, 1995; Pedersen and Larsen, 1989; Sejnoha et al., 1994). Some of these references are discussed at further length when their results are compared with those obtained in this work.

Table 1. Limiting Selectivity ($s^0_{i,1}$) and Isotherm Slope Ratio for the Adsorption of Alkanes C_2–C_5 on Activated Carbon at Depletion Pressure (1.4 atm) and 25°C

	Ethane	Propane	Butane	Pentane
$s^0_{i,1} = \lim_{y_i \to 0} \dfrac{x_i/y_i}{x_1/y_1}$	3.0×10^{1}	2.0×10^{3}	1.5×10^{5}	8.9×10^{6}
$(\partial q/\partial P)_i/(\partial q/\partial P)_1$	1.1×10^{0}	7.6×10^{-1}	4.6×10^{-1}	3.0×10^{-1}

Note: The selectivity of species i in a binary mixture consisting essentially of methane is denoted by $s^0_{i,1}$, and subscript 1 = methane.

Interestingly, the presence of other species in the gas mixture is not necessarily prejudicial for adsorptive storage. An example that ascertains this statement is the concept of ''Enhanced Adsorptive Storage,'' introduced by Talu (1993), where net storage capacity can be increased by an additive intentionally added to the gas stream before charge. The storage enhancement occurs if the additive's impact on the amount of NG adsorbed at depletion pressure is higher than at charge pressure.

Considerable experimental work has been invested on the design and test of economical means of controlling the contaminants that are allowed to enter the onboard storage system. The preferred approach is a carbon bed installed as a filter unit at the refueling station (Bevier et al., 1989; Sejnoha et al., 1994), or as a guard bed placed in line in front of the storage tank (Cook et al., 1996; Strisna et al., 1989). In both cases, regeneration is accomplished by heating the carbon bed.

In spite of the studies just cited, no research work has addressed, from a modeling perspective, the impact of gas composition on the cyclic behavior of ANG storage systems during extended operation. Previous dynamic modeling studies on ANG storage are restricted to methane adsorption (Chang and Talu, 1996; Mota, 1995; Mota et al., 1995, 1997a,b; Sangani, 1990). Usually, large-scale test benches and time-consuming experiments are required to simulate experimentally the cyclic operating conditions expected in a vehicle (Sejnoha et al., 1994). A reliable, predictive multicomponent dynamic model is therefore a highly desirable research objective. This article presents the results of our modeling effort to accomplish this goal.

The article is organized as follows: first, the model employed for multicomponent adsorption equilibrium prediction is described. This constitutes the basis of the dynamic model of the adsorptive storage system. The dynamic model is validated as much as possible by comparison with published experimental data. Particular attention is given to the composition and calorific value of the delivered gas and to performance quantifiers that measure net deliverable capacity as a function of cycle number. Evidence of a cyclic steady state is given. Whenever possible, the numerical results are compared with experimental measurements.

Multicomponent Adsorption Equilibrium

Adsorption equilibrium data are the basis of every adsorption process modeling study. When there are several adsorbates, as in the case of a real NG, the equilibrium composition must be predicted from isotherms for single gases, because the number of experimental measurements required increases exponentially with the number of components.

Unfortunately, even for single-component equilibrium few experimental data are reported in the literature for adsorption of the various components of NG on the same carbon,

covering a large range of pressure and temperature. Although a gravimetric apparatus is being built in our laboratory for this purpose, it was not ready in time to be employed in the present study. In order to overcome the lack of experimental data, multicomponent adsorption equilibrium is predicted by an approach combining the Adsorption Potential (Brunauer, 1945; Dubinin, 1989; Stoeckli, 1995) and the Ideal Adsorbed Solution (IAS) (Myers and Prausnitz, 1965) theories.

This approach was mentioned briefly by Myers (1989) in a review of theories of adsorption in micropores. The author considered the Adsorption Potential theory in the form of the Dubinin–Radushkevich isotherm. Very recently, Stoeckli and coworkers extended the method to the Dubinin–Astakov isotherm (Lavanchy et al., 1996; Stoeckli et al., 1997), and were the first to apply both theories to an adsorption column modeling study (Lavanchy and Stoeckli, 1997). These authors were able to predict breakthrough curves for the binary adsorption of several vapors on activated carbon, under isothermal conditions, using IAS and the Dubinin–Radushkevich isotherm (Lavanchy and Stoeckli, 1997).

In this work, a different form of the characteristic curve is employed and the theory is applied to a gas mixture with several components under nonisothermal conditions. It should be noted that adsorbed-phase nonideality is neglected in the present study and that the generalization of the Adsorption Potential theory has limited capability. Nevertheless, the combined approach is sufficiently accurate to provide a reasonable description of how gas composition affects the dynamic behavior of an adsorptive storage system.

Recently, Chang and Talu (1996) presented a comprehensive study of the behavior of adsorbed methane storage cylinders during discharge, including extensive P-T measurements (measurements of pressure and temperature) taken under realistic dynamic conditions. Their isotherm data for methane adsorption on activated carbon (Figure 2) are the basis of the adsorption equilibrium model employed in the present study. This choice gives the opportunity of assessing how well the dynamic model developed in this work reproduces the experimentally observed behavior, at least for single-gas adsorption.

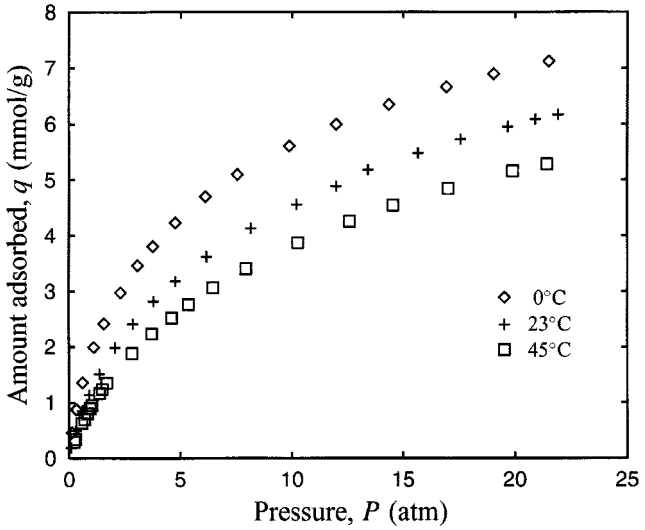

Figure 2. Experimental isotherm data reported by Chang and Talu (1996) for methane adsorption on activated carbon.

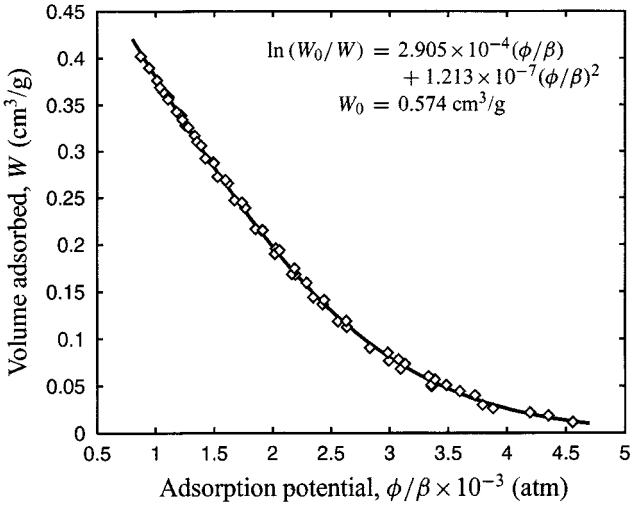

Figure 3. Characteristic curve of adsorption on activated carbon.

The symbols denote the experimental data shown in Figure 2 plotted according to the Adsorption Potential theory; the solid line represents the least-squares fit of Eq. 5.

The analysis of the methane isotherm data on the basis of the Adsorption Potential theory gives rise to a characteristic curve of adsorption on the carbon. The characteristic curve, depicted in Figure 3, is the functional relationship between volume of the adsorbed phase,

$$W \equiv qV_A, \tag{1}$$

and adsorption potential,

$$\phi = R_g T \ln(P_s/P). \tag{2}$$

In this work, vapor pressure, P_s, and adsorbed molar volume, V_A, were calculated according to the following expressions (Dubinin, 1975; Ozawa et al., 1976):

$$P_s = \begin{cases} P_c(T/T_c)^2, & T > T_c \\ P_c^{(1-T_b/T)/(1-T_b/T_c)}, & T < T_c, \end{cases} \tag{3}$$

$$V_A = V_b \exp\left[\alpha_e(T - T_b)\right], \qquad \alpha_e = \frac{\ln(R_g T_c/8P_c V_b)}{T_c - T_b}, \tag{4}$$

where V_b is the adsorbate liquid molar volume at the normal boiling point T_b and α_e is an estimate of the thermal expansion coefficient of the liquefied gas.

We assume that for the hydrocarbons in NG an affinity coefficient β can be used as a shifting factor to bring their characteristic curves on the same carbon into a single curve. Based on the author's past experience on light hydrocarbon adsorption, as a first approximation β can be replaced by the liquid molar volume of the adsorbate at the normal boiling

point, that is, $\beta \approx V_b$. This approximation has been used with success by other authors (Agarwal and Schwarz, 1988; Grant and Manes, 1964, 1966; Reich et al., 1980).

According to the Adsorption Potential theory, the characteristic curve is temperature independent. This premise is fully verified by the experimental data, as demonstrated in Figure 3, and corroborates the applicability of the theory to the carbon under study. Although the functional form of the characteristic curve is adsorbent dependent, expressing the logarithm of W as a truncated series development of the scaled adsorption potential, ϕ/β, has proved very versatile in fitting characteristic curves of various degrees of nonlinearity (Ozawa et al., 1976):

$$\ln(W_o/W) = \sum_{i=1}^{n} k_i(\phi/\beta)^i. \tag{5}$$

Furthermore, a second-order polynomial ($n = 2$) usually gives a close fit of the experimental data, as can be seen in Figure 3. From this curve the single-component adsorption isotherms for the various components can be generated quite easily. The isotherms shown in Figure 1 were obtained by applying this procedure to the experimental methane adsorption data given in Figure 2.

In order to embed the IAS method is the dynamic simulation model, the spreading pressure of the gas mixture, Π, is treated as a dependent variable, just like temperature or partial pressure of each adsorbate. The equation that Π must ultimately satisfy is the condition

$$\sum_{i=1}^{\mathrm{NC}} x_i = 1, \tag{6}$$

where the x_i are the adsorbed-phase mole fractions derived from the values of Π, temperature, and partial pressures. The x_i values are computed as follows. First, the pressures P_i^0, at which the pure-component adsorption equilibria yield the same value of Π, are calculated from the Gibbs adsorption equation:

$$\int_0^{P_i^0} q_i^0(P,T)\, d\ln P = \frac{\Pi A}{R_g T}, \qquad i = 1, \ldots, \mathrm{NC} \quad (\text{const. } T), \tag{7}$$

where $q_i^0(P,T)$ is the adsorption isotherm of pure component i. Then the basic equation of IAS is employed to calculate x_i:

$$x_i = Py_i/P_i^0(\Pi), \qquad i = 1, \ldots, \mathrm{NC}. \tag{8}$$

Once the correct value of Π has been determined, the adsorbed-phase composition is computed by the following expression:

$$\frac{1}{q} = \sum_{i=1}^{\mathrm{NC}} \frac{x_i}{q_i^0(P_i^0,T)}, \quad q_i = x_i q, \qquad i = 1, \ldots, \mathrm{NC}. \tag{9}$$

From the definition of adsorption potential, Eqs. 7 and 8 can be rewritten as

$$\int_{\phi_i^0/\beta_i}^{\infty} W(\phi^*)\, d\phi^* = \Pi_i^* \equiv (V_A/\beta)_i \Pi A, \quad \phi_i^0 \equiv \phi_i(P_i^0,T), \quad i = 1, \ldots, \mathrm{NC} \quad (\text{const. } T), \tag{10}$$

$$x_i = \exp\left(\frac{\phi_i^0 - \phi_i}{R_g T}\right) = \frac{y_i P}{P_{s,i}} \exp\left(\frac{\phi_i^0}{R_g T}\right), \quad i = 1, \ldots, \mathrm{NC}. \tag{11}$$

The advantage of rewriting Eq. 10 in terms of ϕ is that all species share the same integral function (the lefthand side of the equation). This means that if the characteristic curves can be superposed using shifting factors, then the spreading pressure for the various species can be derived from a single curve also. In this sense, Π^* can be viewed as a scaled spreading pressure.

The author has observed that if the experimental characteristic curve can be fitted well by Eq. 5 with $n = 2$, then Π^* also can be approximated by a similar expression:

$$\ln(\Pi_o^*/\Pi^*) = s_1(\phi/\beta) + s_2(\phi/\beta)^2, \qquad s_1 > 0,\ s_2 > 0. \tag{12}$$

Figure 4 shows the least-squares fit of Eq. 12 to the values of Π^* obtained by solving numerically Eq. 10 using an adaptive quadrature procedure. As can be judged from the figure, the agreement between the fitted curve and the data is excellent. In fact, the fitted curve nearly interpolates the data. The most advantageous feature of Eq. 12 is that it can be rewritten explicitly for the scaled adsorption potential:

$$\phi/\beta = \frac{s_1}{2s_2}\left[\sqrt{1 + (4s_2/s_1^2)\ln(\Pi_o^*/\Pi^*)} - 1\right]. \tag{13}$$

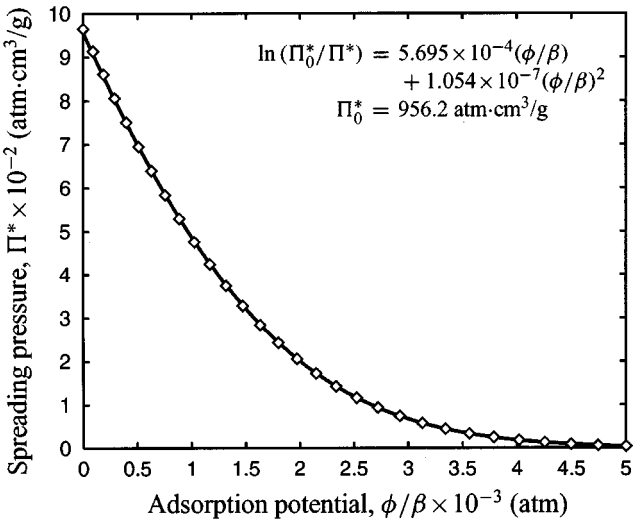

Figure 4. Scaled spreading pressure, $\Pi^* \equiv (V_A/\beta)\Pi A$, as a function of scaled adsorption potential, ϕ/β, for the carbon under study.

The symbols denote values of Π^* obtained by solving Eq. 10 numerically using an adaptive quadrature procedure; the solid line is the least-squares fit of Eq. 12.

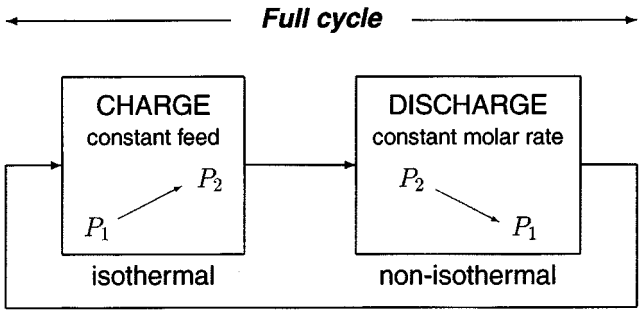

Figure 5. Simulated cyclic operation of an ANG onboard storage system; P_1 = depletion pressure; P_2 = charge pressure.

This makes the computation of x_i an easy task, and reduces considerably the computational overhead introduced by the IAS method.

Problem Formulation and Theoretical Model

In order to assess the impact of gas composition on net deliverable capacity, the dynamic behavior of an onboard storage reservoir is modeled as a series of consecutive cycles. Each cycle is a two-step process consisting of a charge with a fixed-composition gas mixture, followed by discharge at a constant molar flow rate until depletion pressure is attained. This cyclic operation is depicted in Figure 5.

Discharge phase

The model for the discharge phase is an extension to multicomponent adsorption of previous work (Chang and Talu, 1996; Mota, 1995; Mota et al., 1997a,b) on modeling the dynamic behavior of methane adsorptive storage cylinders under similar conditions.

In an onboard ANG storage tank the discharge flow rate is dictated by the power requirements of the engine. The discharge rates involved in this process are sufficiently slow to ensure the validity of the following assumptions: pressure is uniform within the cylinder; there is instantaneous equilibrium between gas and adsorbed phase; intraparticle gradients are negligible; the temperature of gas and particle are the same at each point in the bed. These assumptions justify the adoption of an equilibrium model at the particle level.

In spite of the process slowness, experimental work showed that under realistic discharge conditions the consumed heat of desorption is only partially compensated by the wall thermal capacity and by the heat transferred from the surrounding environment (Chang and Talu, 1996). As a result, a radial temperature profile develops in the medium, the major temperature drop occurring at the center of the bed.

The cylinder that is modeled in this work is sufficiently long so that the small axial temperature gradient induced by the front and rear faces has negligible impact on overall system dynamics. The convective phenomena driven by natural convection inside the cylinder, which would be potential candidates for increasing the complexity of the model, are also negligible (Mota, 1995; Sangani, 1990). Thus, every differential volume of the carbon bed at the same radial location contributes with the same amount of gas to the overall discharge rate, regardless of its axial position. According to these assumptions the spatial dimensionality of the problem is reduced substantially, since only the radial profile needs to be taken into account.

The differential material balance for species i ($i = 1, \ldots,$ NC) on a cylindrical shell element of the reservoir can be written as

$$\epsilon \frac{\partial c_i}{\partial t} + \rho_b \frac{\partial q_i}{\partial t} - \epsilon \nabla \cdot (D_{e,i} c \nabla y_i) + y_i \tilde{F} = 0, \qquad (14)$$

where $\tilde{F}(t,r)$ is the local contribution to the overall molar discharge rate per unit reservoir volume, and

$$\nabla \cdot (D_{e,i} c \nabla y_i) = \frac{1}{r} \frac{\partial}{\partial r} \left(r D_{e,i} c \frac{\partial y_i}{\partial r} \right). \qquad (15)$$

The preceding material balances are subjected to boundary conditions

$$\partial y_i / \partial r = 0 \qquad \text{for} \qquad r = 0,\ R_o. \qquad (16)$$

Given that pressure remains uniform within the cylinder, the temperature profile induces radial concentration gradients in both adsorbed and gas phases. The latter are smeared by molecular diffusion in the bulk phase, which is modeled by the third term of Eq. 14. As will be shown later, the gas phase is always very rich in methane, even after a large number of cycles. For multicomponent diffusion in a mixture consisting essentially of component 1 (methane), the Stefan–Maxwell equations can be simplified giving rise to handy expressions for the effective diffusion coefficients $D_{e,i}$ (Wilke, 1950; Hirschfelder et al., 1954):

$$\frac{1 - y_1}{\tau D_{e,1}} = \sum_{i=2}^{\text{NC}} \frac{y_i}{D_{1i}}, \qquad D_{e,i} = D_{1i}/\tau \qquad (i \geq 2). \quad (17)$$

The symbol D_{ij} denotes the molecular diffusion coefficient for the binary pair $i-j$ and τ is the bed tortuosity factor. The D_{ij} are estimated by the Wilke-Lee equation (Reid et al., 1977).

The local contribution $\tilde{F}$ varies along r in order to make pressure uniform in the cylinder and to satisfy the overall material balance over the cross section of the cylinder:

$$2\pi L \int_0^{R_o} \tilde{F}(t,r)\, r dr = F, \qquad (18)$$

where F is the imposed overall molar discharge rate. Most of the gas is stored in adsorbed form, whose concentration depends strongly on temperature; this is the main reason why $\tilde{F}$ changes with r. The constraint (Eq. 18) may seem complicated to solve but, as is shown later, it can be handled easily.

The energy equation, applied to the same differential volume, yields

$$\left[\rho_b C_s + C_g(\epsilon c + \rho_b q)\right]\frac{\partial T}{\partial t} - \epsilon\frac{dP}{dt} + \rho_b\sum_i(-\Delta H)_i\frac{\partial q_i}{\partial t} - \nabla\cdot(\lambda_e\nabla T) = 0, \quad (19)$$

where C_s and C_g are the carbon and gas heat capacities, respectively, $(-\Delta H)_i$ is the heat of adsorption of species i, and λ_e is the effective thermal conductivity of the carbon bed. As a first approximation, the heat capacity of the adsorbed phase is considered equal to that of the gas with the same composition. Equation 19 is subjected to boundary conditions

$$\partial T/\partial r = 0 \qquad \text{for} \qquad r = 0, \quad (20)$$

$$\left(1+\frac{e_w}{2R_o}\right)e_w C_w\frac{\partial T}{\partial t} + \lambda_e\frac{\partial T}{\partial r} = \left(1+\frac{e_w}{R_o}\right)h_w(T_0 - T) \qquad \text{for} \qquad r = R_o. \quad (21)$$

The latter condition is an energy balance on the steel cylinder wall; it cannot be neglected, due to its large thermal capacity. The symbols e_w, C_w, and h_w represent wall properties (thickness, volumetric heat capacity, and natural convection heat-transfer coefficient at the external surface, respectively), and T_0 is ambient temperature. The temperature profile along the wall thickness can be neglected because the wall is relatively thin (≈ 0.5 cm) and its thermal conductivity is much higher than that of the packed bed. Two heat transfer mechanisms are taken into account: conduction to the packed bed, and natural convection from the outside air.

Charge phase

The charge phase can be carried out in several ways. However, only those in which the detrimental effect of the heat of adsorption is eliminated are likely to be adopted in practice. For a fast fill at the refueling station, the most economical strategy seems to be an external NG recycle loop that removes the released heat of adsorption and transfers it to the environment across an air-cooled heat exchanger (BeVier et al., 1989; Jasionowski et al., 1992). Alternatively, in fleet applications the vehicles can be charged over a long period, for example, overnight, which provides enough time to dissipate the heat of adsorption (Parkyns and Quinn, 1995; Chang and Talu, 1996).

Both approaches give rise to isothermal charges in which, as a first approximation, the storage vessel can be viewed as a perfectly mixed adsorber. The reason for this simplification is that at the end of the charge step the concentration profiles in the storage tank have been smeared by the recirculation loop effect or the very long filling time. These assumptions suggest that an isothermal lumped-based model can be employed for the charge phase. In this case, the material balances are very simple and can be expressed either in differential or algebraic form. The algebraic formulation is retained here, since the main goal is to compute the conditions prevailing in the carbon bed before the next discharge is started.

At the end of the discharge, which coincides with the end of the cycle, the residual amount of each component left in storage per unit reservoir volume is computed from

$$S_i = \left(2/R_o^2\right)\int_0^{R_o}(\epsilon c_i + \rho_b q_i)r\,dr \qquad \text{at depletion.} \quad (22)$$

Then, the following set of lumped material balances is solved in order to compute the initial conditions for the next discharge:

$$\epsilon c_i + \rho_b q_i = S_i + z_i Q \qquad (i = 1, \ldots, \text{NC}), \quad (23)$$

with

$$P = P_2 \qquad \text{and} \qquad T = T_0, \quad (24)$$

where Q is the amount of gas stored in the cylinder during charge, and z_i is the mole fraction of species i in the charge gas. In this formulation, Q is an unknown that must be computed along with the new discharge initial conditions.

Numerical Solution

The easiest way to handle the integral constraint (Eq. 18) is to modify Eq. 14 so that the constraint is satisfied implicitly. This is computationally more efficient than the alternative approach of employing a single pressure value along r, in order to satisfy the uniform pressure condition, and calculating at each time step the pressure drop that satisfies Eq. 18.

The basic idea employed here is to distribute the imposed molar discharge rate evenly over the whole cylinder and then to equilibrate the pressure by a flow mechanism governed by Darcy's law. If the pressure equilibration step is sufficiently fast, the uniform pressure condition is always verified. In mathematical terms, the original material balances (Eq. 14) are rewritten as

$$\epsilon\frac{\partial c_i}{\partial t} + \rho_b\frac{\partial q_i}{\partial t} - \epsilon\nabla\cdot(D_{e,i}c\nabla y_i) + y_i(\bar{F} + F') = 0, \quad (25)$$

where $\bar{F} \equiv F/(\pi R_o^2 L)$ is the imposed molar discharge rate per unit reservoir volume and $F'(t,r)$ is the deviation from $\bar{F}$. Besides forcing the pressure to be uniform, F' must, according to Eq. 18, satisfy the integral constraint

$$\int_0^{R_o}F'(t,r)\,r dr = 0. \quad (26)$$

The pressure equilibration step is introduced in the model by setting

$$y_i F' \equiv -\alpha\nabla\cdot(c_i\nabla P). \quad (27)$$

Hence, the material balances that are actually solved are

$$\epsilon\frac{\partial c_i}{\partial t} + \rho_b\frac{\partial q_i}{\partial t} - \nabla\cdot(\epsilon D_{e,i}c\nabla y_i + \alpha c_i\nabla P) + y_i\bar{F} = 0, \quad (28)$$

subjected to boundary conditions

$$\partial c_i/\partial r = 0 \qquad \text{for} \qquad r = 0,\ R_o. \tag{29}$$

A physical meaning can be given to α. This parameter can be viewed as the ratio K/μ, where K is the equivalent to a bed permeability, and μ is gas viscosity. It is readily seen that Eq. 27 always satisfies the integral constraint (Eq. 26). Therefore, the only requirement is that α be large enough to ensure uniform pressure in the cylinder at any instant. However, an excessively high value renders the other terms in Eq. 28 insignificant. In practice, α values based on representative magnitudes of K and μ ($K \sim 10^{-10} - 10^{-9}$ m^2, $\mu \sim 10^{-5}$ kg m^{-1}s^{-1}) give the desired effect.

The equations were solved numerically by the finite-volume method and a modified version of a public domain differential/algebraic system solver (Mota et al., 1997c). Preliminary runs were carried out in order to assess the accuracy of the computed solution. It was found that 15 equally spaced grid points were sufficient to ensure that the numerical results are independent of spatial resolution to within the accuracy requested (10^{-4} relative error tolerance).

Given that the code written for the discharge phase was found to be computationally efficient, it also was employed to solve the charge-phase model. Instead of solving Eqs. 22–24, the charge phase was simulated as as two-step process that gives the same results: (1) thermal equilibration with the surroundings, in which the discharge model is solved with $\bar{F} = 0$ until uniform temperature is attained in the cylinder; and (2) isothermal pressurization to the charge-pressure value. The latter step is solved with $y_i\bar{F}$ replaced by $-z_i\bar{F}$ in Eq. 28 and with the energy equation inactive.

Results and Discussion

Model validation for methane adsorption

The discharge phase model is validated for single-gas adsorption by comparing its predictions with the measurements, reported by Chang and Talu (1996), of pressure history and temperature profiles in an adsorbed methane cylinder during discharge. The comparison can be made because the dynamic experiments employed the same carbon on which the methane isotherm data of Figure 2 were measured. As shown in Figures 6 and 7, the numerical results are in close agreement with the experimental measurements.

Our model predicts the temperature field (Figure 7) with about the same accuracy as that of the simpler model proposed by Chang and Talu (1996). The pressure history shown in Figure 6, however, is predicted with higher accuracy by the present model. According to Chang and Talu, the discrepancy between their model and the experiment was caused by the gas-phase accumulation term, which was not taken into account during the solution of the model, although it was subsequently included in the final results in an approximate way. Our results confirm their conjecture, because gas-phase accumulation is fully taken into account in the present model.

Figure 7 illustrates the impact of the heat of desorption on ANG storage. In this case, the storage system delivers only 80% of the amount of methane delivered in isothermal conditions. The nonisothermal operation of ANG storage systems is a factor determining the feasibility of this storage technology in mobile applications and has been addressed by several authors (Chang and Talu, 1996; Mota, 1995; Mota et al., 1997a,b; Remick and Tiller, 1986).

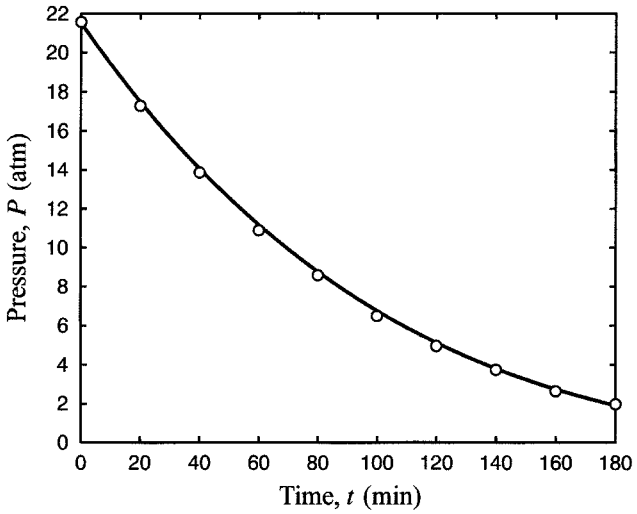

Figure 6. Pressure history in an adsorbed methane storage cylinder during discharge at constant molar flow rate.

Comparison between experimental data (symbols) reported by Chang and Talu (1996) and model predictions (solid line). $L = 74$ cm; $R = 10$ cm; carbon weight = 15.78 kg; $P_2 = 21$ bar; $P_1 = 1.66$ bar; discharge rate = 6.7 dm^3/min (ambient conditions).

Multicomponent results

The gas mixture employed in the multicomponent simulations is described in Table 2, and characterizes the Algerian

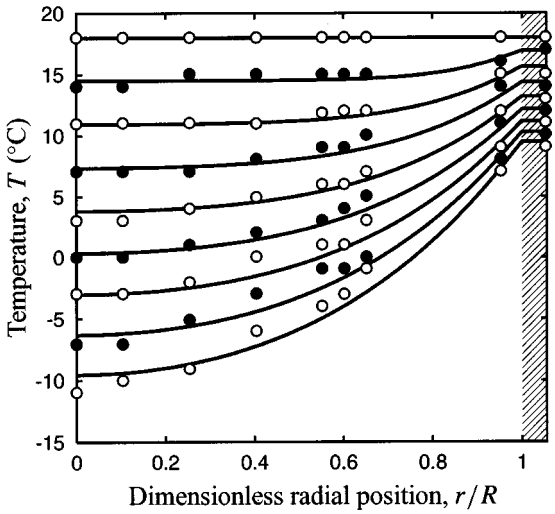

Figure 7. Radial temperature profiles in an adsorbed methane storage cylinder as a function of time during discharge at constant molar flow rate.

Comparison between experimental data (symbols) reported by Chang and Talu (1996) and model predictions (solid line). Sampling interval = 20 min; $L = 74$ cm; $R = 10$ cm; carbon weight = 15.78 kg; $P_2 = 21$ bar; $P_1 = 1.66$ bar; discharge rate = 6.7 dm^3/min (ambient conditions).

Table 2. Composition and Thermodynamic Properties of the Algerian Natural Gas from the Hassi R'Mel Well that Supplies Portugal

Component	CH_4	C_2H_6	C_3H_8	C_4H_{10}	C_5H_{12}	N_2
Mole fraction	0.840	0.076	0.020	0.007	0.003	0.054
P_c (atm)	45.4	48.2	41.9	37.5	33.3	33.5
T_c (K)	190.6	305.4	369.8	425.2	469.6	126.2
V_b (cm^3/mol)	37.7	54.9	74.5	94.8	114.0	34.8
T_b (K)	111.7	184.5	231.1	272.7	309.2	77.4
ΔH_c (kJ/mol)	803.1	1429	2045	2660	3274	—

NG from the Hassi R'Mel well that supplies the author's country. Table 3 lists the values of the main parameters employed in the numerical simulations. The discharge flow rate considered, $\bar{F} = 2\times10^{-7}$ mol/cm^3·s, gives a discharge duration of about 4 h for nonisothermal operation of the storage cylinder on pure methane. Its value is representative of the demand rate for a compact-class car on the EPA city cycle (gasoline consumption of 7 L/100 km). Depletion pressure is 1.4 atm, while charge pressure is 35 atm. Upper pressure limits in the range 35–40 atm are the more commonly accepted charge-pressure values.

In a charge step governed by Eqs. 22–24, the various species are stored in the cylinder in an amount proportional to their mole fraction in the NG supplied. If the vehicle is always refueled with the same gas mixture, the storage cylinder will approach a cyclic steady state on extended operation. When the cyclic steady state is reached, net charge capacity and net deliverable capacity are identical: the gas stored in the cylinder during charge is fully delivered to the motor during discharge. Furthermore, under cyclic steady-state operation the overall composition of the gas delivered by the cylinder in each discharge is the same as that of the NG supplied by the refueling station. This is true regardless of the continuous change with time of the instantaneous composition of the gas delivered by the cylinder. Thus, under cyclic steady-state operation, the total amount of species i delivered by depressurizing the cylinder from P_2 down to P_1 is

$$z_i Q^{(\infty)}, \tag{30}$$

where $Q^{(\infty)}$ is the total amount of gas delivered by the cylinder under cyclic steady-state conditions and z_i is the species mole fraction in the NG supplied by the refueling station (Table 2). This fact suggests that the net deliverable capacity of an ANG storage system can be conveniently measured in terms of a dynamic efficiency, η, which for component i is defined as

Table 3. Data Employed in Numerical Simulations

$C_g = 36.0$ mol·K	$P_l = 1.4$ atm
$C_s = 1.05$ J/g·K	$R_o = 10$ cm
$C_w = 3.92$ J/cm^3·K	$T_0 = 20$°C
$e_w = 0.55$ cm	$\epsilon = 0.5$
$\bar{F} = 2\times10^{-7}$ mol/cm^3·s	$\lambda_e = 2.1$ mJ/cm·s·K
$L = 74$ cm	$\rho_b = 0.481$ g/cm^3
$P_h = 35$ atm	$\tau = 3.0$

$$\eta_i = \frac{\text{amount of species } i \text{ delivered under dynamic conditions}}{(\text{amount of pure methane delivered isothermally})\cdot z_i}. \tag{31}$$

With this definition, the η_i converge to a single point at the cyclic steady-state, whose value is

$$\eta^{(\infty)} = \frac{Q^{(\infty)}}{\text{amount of pure methane delivered isothermally}}. \tag{32}$$

This feature is depicted in Figure 8. Note that η takes into account the loss in capacity due to both the composition of the gas mixture and the nonisothermal operation of the discharge step.

The mole fractions shown in Figure 9 refer to the overall composition of the gas delivered by the cylinder during discharge. They are expressed as

$$\bar{\bar{y}}_i = \left(\int_0^{t_d}\int_0^{R_o} y_i \tilde{F}\, r\, dr\, dt\right) \Big/ \left(\int_0^{t_d}\int_0^{R_o} \tilde{F}\, r\, dr\, dt\right), \tag{33}$$

where t_d is the discharge duration, which is a function of the cycle number due to the gradual loss in capacity. The double-overbar is a notation to make clear that the variable is averaged both in time and in space. In practice, the $\bar{\bar{y}}_i$ are more conveniently computed from the overall material balance to the discharge step:

$$\bar{\bar{y}}_i = S_i^{(n)} + z_i Q^{(n)} - S_i^{(n+1)}, \tag{34}$$

where the integer superscript refers to the cycle number.

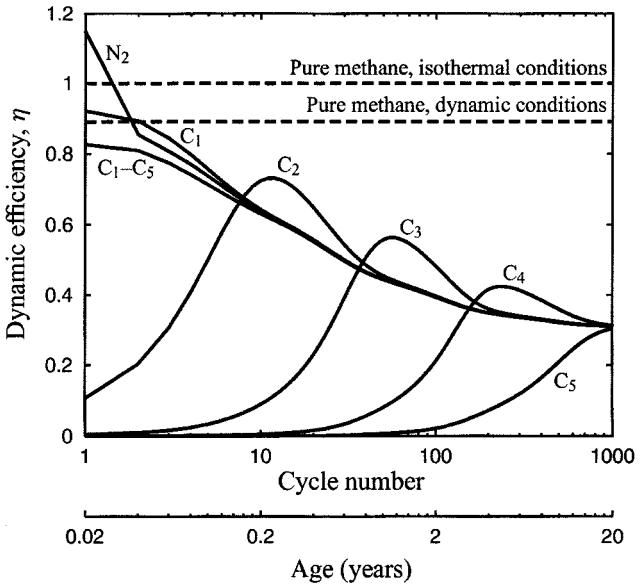

Figure 8. Dynamic efficiency, η, as a function of cycle number for the ANG storage cylinder.

C_1: methaane; C_2: ethane; C_3: propane; C_4: butane; C_5: pentane; C_1–C_5 identifies the total hydrocarbon dynamic efficiency, η_{1-5}.

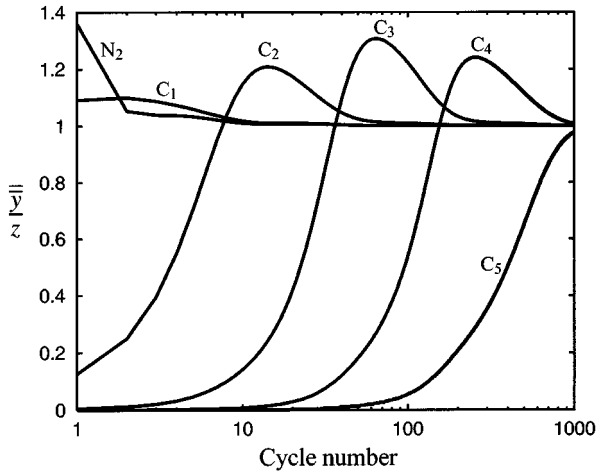

Figure 9. Overall composition of gas delivered by the ANG storage cylinder during discharge as a function of cycle number.

The species mole fraction in the gas delivered by the cylinder is denoted by $\bar{\bar{y}}$, and z is its mole fraction in the NG supplied by the refueling station (Table 2). C_1: methane; C_2: ethane; C_3: propane; C_4: butane; C_5: pentane.

Figure 8 shows that, for the gas mixture considered in this study, several cycles are necessary before a cyclic steady state is reached, starting from the first cycle with an empty cylinder. A secondary horizontal axis has been added to the figure, based on an average annual number of 50 refills of the storage vessel for a regular city vehicle. For the particular gas composition considered in this study the cyclic steady state is not attained during the expected physical life of the storage reservoir.

Initially, $\bar{\bar{y}}_i$ increases continuously with cycle number, reaches a maximum at an intermediate cycle, and then decreases until it stays constant and equal to z_i (Figure 9). A similar trend is observed for the individual dynamic efficiencies, but in their case they converge to the single cyclic steady-state value, $\eta^{(\infty)}$ (Figure 8). The only exceptions to this general rule are the curves for methane and nitrogen, which are the less strongly adsorbed species. Their dynamic efficiencies converge to the cyclic steady-state value as monotonically decreasing functions of cycle number. For practical purposes, nitrogen can be considered a nonadsorbable gas at ambient temperature.

According to Figure 8, the number of cycles elapsed until $\bar{\bar{y}}_i$ is constant and equal to z_i is an increasing function of the hydrocarbon molecular weight. The reason for this trend is that, as the number of cycles increases, the more strongly adsorbed components progressively displace the less strongly adsorbed ones from the adsorbed phase to the gas phase where there is no competition for storage between species.

Figure 8 shows that $\bar{\bar{y}}_i$ exceeds z_i at intermediate cycles. The peak of the $\bar{\bar{y}}_i$ curve is shifted to a later cycle with increasing hydrocarbon molecular weight. A similar phenomenon is observed in multicomponent adsorption-column dynamics. It is commonly referred to as roll-up or roll-over and alludes to humps on the breakthrough curves, where the outlet concentration exceeds the feed concentration (Yang, 1987). This behavior is, once again, caused by the displacement of a weaker adsorbate by a stronger one. Since the volumetric percentage of alkanes in NG is in general a smooth decreasing function of their molecular weight, the peaks in the $\bar{\bar{y}}$ curves are well spaced along the cycle–number axis. Nevertheless, the maximum value attained by $\bar{\bar{y}}_i$ never exceeds z_i by more than 20%, and for most cycles is below it. Thus, the gas phase is always very rich in methane regardless of the cycle number.

Despite the complex dependency of η_i on cycle number, the total hydrocarbon dynamic efficiency, η_{1-5}, is clearly a monotonically decreasing function of cycle number until the cyclic steady state is reached. Notice that η_{1-5} is defined as

$$\eta_{1-5}=\frac{\text{total amount of HCs delivered under dynamic conditions}}{(\text{amount of pure methane delivered isothermally})\cdot\Sigma z_i}, \tag{35}$$

so that it converges to $Q^{(\infty)}$ as the other η_i do. Another interesting feature, depicted in Figure 8, is that the cycle where the increasing part of the η_{i+1} curve intersects η_{1-5} is always very close to the cycle where the η_{1-5} curve is joined by η_i.

Regarding the NG considered in the present work, which has 90% methane, the results show that there is a drastic reduction in net deliverable capacity with cyclic operation. Before leveling off, the total hydrocarbon capacity loss depends linearly on the logarithm of the number of cycles. This is in qualitative agreement with the experimental observations of Golovoy and Blais (1983) for 1,000 cycles of operation of an ANG cylinder. These authors observed a capacity decrease of 22% after 100 cycles of operation on a NG containing 2.6% impurities. According to Parkyns and Quinn (1995), the latter author performed cyclic testing with a number of different carbons on Canadian NG and also observed significant losses in adsorption capacity. Furthermore, the leveling off of capacity was observed when the cyclic testing was prolonged sufficiently. This is experimental evidence of the cyclic steady-state operation.

In another experimental study, Pedersen and Larsen (1989) observed a capacity loss of more than 50% using an NG with 8.9% impurities. Given that η represents a relative loss in deliverable capacity, its value should be more dependent on gas composition than on the adsorbent. Hence, although the carbon tested by these authors is different from the one considered in the present study, one is tempted to compare both results because the two NGs have nearly the same amount of impurities. When this is done, both results are seen to be in fairly good agreement. For comparison purposes, one should take into account that the storage system modeled here does not operate isothermally, so the loss in net deliverable capacity is increased by about 10% due to nonisothermal operation. This extra penalty is identified in Figure 8 by the difference between the two horizontal dotted lines, which compare the dynamic efficiencies for isothermal and nonisothermal operations on pure methane.

Figure 10 compares the histories of temperature and adsorbed-phase mole fractions, inside the cylinder during discharge, for the first cycle and for the cyclic steady state. The curves refer to lumped values obtained by averaging the vari-

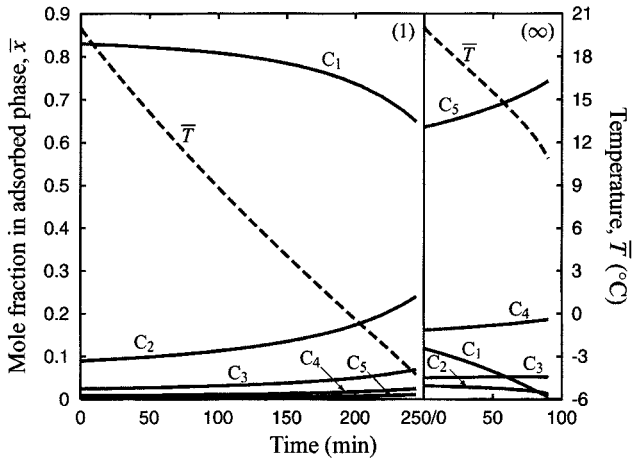

Figure 10. Histories of temperature and adsorbed-phase mole fractions in the ANG storage cylinder for the first cycle (1) and for the cyclic steady state (∞).

The curves correspond to lumped values obtained by averaging the variables over the cross section of the cylinder according to Eq. 36. C_1: methane; C_2: ethane; C_3: propane; C_4: butane; C_5: pentane.

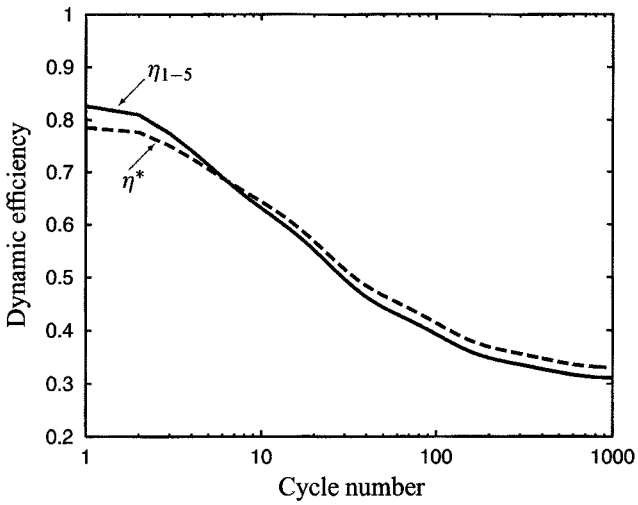

Figure 11. Dynamic efficiencies for total hydrocarbon net deliverable capacity, η_{1-5} and η^*, as a function of cycle number for the ANG storage cylinder.

able over the cross section of the cylinder as follows:

$$\bar{\phi}(t) = \left(2/R_o^2\right)\int_0^{R_o}\phi(t, r)\, rdr. \tag{36}$$

The difference in the results obtained for the first cycle and for the cyclic steady state is noticeable. If the discharge flow rate is held constant, discharge duration decreases with cycle number. This is a direct consequence of the loss in storage capacity due to the gradual filling of the micropore volume with the higher molecular-weight hydrocarbons that remain adsorbed at depletion pressure. When the cyclic steady state is reached, pentane is clearly the species that is more adsorbed. In fact, its mole fraction in the adsorbed phase is at the same level as that of methane in the first cycle.

As the number of cycles increases, the adsorbed phase is enriched with the more strongly adsorbed hydrocarbons, and these have higher heats of desorption than methane. However, they desorb less during discharge. The net effect is that the slope of the temperature history curve remains nearly insensitive to the cycle number, as shown in Figure 10.

In real vehicle operation the discharge flow rate depends on the calorific value of the gas mixture, and the higher molecular weight hydrocarbons have quite substantial calorific values, as they are fuels also. However, this fact was not taken into account in the definition of η. In order to model the dynamic behavior of a storage system that is subjected to a constant calorific discharge rate, the constraint expressed by Eq. 18 must be replaced by

$$2\pi L\int_0^{R_o}\left[\sum_i (\Delta H_c)_i y_i(t, r)\right]\tilde{F}(t, r)\, rdr = (\Delta H_c)_{\mathrm{CH_4}}\cdot F, \tag{37}$$

where $(\Delta H_c)_i$ is the molar heat of combustion of species i (see Table 2). An appropriate performance quantifier that takes into account the true calorific value of the gas mixture delivered by the storage system is a modified dynamic efficiency defined as

$$\eta^* = \frac{\Sigma_i(\text{amount of species } i \text{ delivered under dynamic conditions})\cdot(\Delta H_c)_i}{(\text{amount of methane delivered under isothermal conditions})\cdot(\Delta H_c)_{\mathrm{CH_4}}}. \tag{38}$$

Figure 11 shows both dynamic efficiencies, η_{1-5} and η^*, as a function of cycle number. The two curves are very close to each other, showing that the dynamic efficiencies defined either on a molar basis or a calorific-value basis are similar quantifiers. This fact could be anticipated by observing Figure 9. The gas phase is always very rich in methane; hence, the impact of gas composition on the calorific value of the gas mixture delivered by the storage system is not significant.

Conclusions

A detailed mathematical model has been developed in order to study the impact of gas composition on the cyclic behavior of ANG reservoirs. Although the results presented concern one carbon and a single gas composition, other NG compositions give rise to the same qualitative behavior.

Performance levels required for commercial viability of onboard ANG storage have already been achieved with methane under isothermal conditions. However, there are other species besides methane in a real NG. The results given here demon-

trate that any commercial application of this storage technology must provide an economical means of removing the higher molecular-weight hydrocarbons and other highly adsorbed species from the gas stream before charging the storage vessel.

Acknowledgments

This work was partly supported by Fundação para a Ciência e Tecnologia through Program PRAXIS XXI (PCEX/C/QUI/109/96).

Notation

c = gas concentration, $\text{mol}\cdot\text{cm}^{-3}$
L = cylinder length, cm
NC = number of components
P_1 = depletion pressure, atm
P_2 = charge pressure, atm
P_c = critical pressure, atm
q = amount adsorbed, $\text{mol}\cdot\text{g}^{-1}$
r = radial coordinate in cylinder, cm
R_g = ideal gas constant, 8.3144 $\text{J}\cdot\text{mol}^{-1}\cdot\text{K}^{-1}$
R_o = cylinder radius, cm
T_c = critical temperature, K
y = mole fraction in gas phase
ϵ = porosity of carbon bed
ρ_b = bulk density of carbon bed, $\text{g}\cdot\text{cm}^{-3}$

Literature Cited

Agarwal, R. K., and J. Schwarz, "Analysis of High Pressure Adsorption of Gases on Activated Carbon by Potential Theory," *Carbon*, **26**, 873 (1988).

BeVier, W. E., J. T. Mullhaupt, F. Notaro, I. C. Lewis, and R. E. Coleman, "Adsorbent-Enhanced Methane Storage for Alternate Fuel Powered Vehicles," SAE Future Transportation Technology Conf. and Exposition, Vancouver, B.C., Canada (1989).

Brunauer, S., *The Adsorption of Gases and Vapours*, Oxford and Princeton Univ. Press, Princeton, NJ (1945).

Chang, K. J., and O. Talu, "Behavior and Performance of Adsorptive Natural Gas Storage Cylinders During Discharge," *Appl. Thermal Eng.*, **16**, 359 (1996).

Cook, T. L., C. Komodromos, D. F. Quinn, and S. Ragan, "A Low Pressure Natural Gas Vehicle Storage System," Windsor Workshop on Alternative Fuels, Toronto, Ont., Canada (1996).

Cook, T. L., C. Komodromos, D. F. Quinn, and S. Ragan, "Adsorbent Storage for Natural Gas Vehicles," *Carbon Materials for Advanced Technologies*, T. Burchell, ed., Elsevier, Amsterdam (1999).

Czepirski, L., "Some Aspects of a Sorbent-Containing Storage System for Natural Gas," *Indian J. Technol.*, **29**, 266 (1991).

Dubinin, M. M., *Progress Surface and Membrane Science*, D. A. Cadenhead et al., eds., Vol. 9, Chap. 1, Academic Press, New York (1975).

Dubinin, M. M., *Carbon*, **27**, 457 (1989).

Golovoy, A., and E. J. Blais, "Natural Gas Storage on Activated Carbon," *Alternative Fuels for Special Ignition Engines, SP-559 SAE Conf. Proc.*, Warrendale, PA, p. 47 (1983).

Grant, R. J., and M. Manes, "Correlation of Some Gas Adsorption Data Extending to Low Pressures and Supercritical Temperatures," *Ind. Eng. Chem. Fundam.*, **3**, 221 (1964).

Grant, R. J., and M. Manes, "Adsorption of Binary Hydrocarbon Gas Mixtures on Activated Carbon," *Ind. Eng. Chem. Fundam.*, **5**, 490 (1966).

Hirschfelder, J. O., C. F. Curtiss, and R. B. Bird, *Molecular Theory of Gases and Liquids*, Wiley, New York (1954).

Jasionowski, W. J., A. J. Tiller, J. A. Fata, J. M. Arnold, S. W. Gauthier, and Y. A. Shikari, "Charge/Discharge Characteristics of High-Capacity Methane Adsorption Storage Systems," Int. Gas Research Conf., Tokyo (1989).

Kasuh, T., K. Okawa, and T. Maeda, "Low Pressure Storage Concept for Natural Gas Fueled Vehicles," *Proc. Int. Gas Res. Conf.*, p. 485 (1992).

Lavanchy, A., M. Stöckli, C. Wirz, and F. Stoeckli, "Binary Adsorption of Vapours in Active Carbons Described by the Dubinin Equation," *Adsorp. Sci. Technol.*, **13**, 537 (1996).

Lavanchy, A., and F. Stoeckli, "Dynamic Adsorption of Vapour Mixtures in Active Carbon Beds Described by the Myers-Prausnitz and Dubinin Theories," *Carbon*, **35**, 1573 (1997).

Mota, J. P. B., "Modélisation des Transferts Couplés en Milieux Poreux," Thèse de Doctorat, Institut National Polytechnique de Lorraine, Nancy, France (1995).

Mota, J. P. B., E. Saatdjian, D. Tondeur, and A. E. Rodrigues, "A Simulation Model of a High-Capacity Methane Adsorptive Storage System," *Adsorption*, **1**, 17 (1995).

Mota, J. P. B., A. E. Rodrigues, E. Saatdjian, and D. Tondeur, "Charge Dynamics of a Methane Adsorption Storage System: Intraparticle Diffusional Effects," *Adsorption*, **3**, 117 (1997a).

Mota, J. P. B., A. E. Rodrigues, E. Saatdjian, and D. Tondeur, "Dynamics of Natural Gas Adsorption Storage Systems Employing Activated Carbon," *Carbon*, **35**, 1259 (1997b).

Mota, J. P. B., E. Saatdjian, D. Tondeur, and A. E. Rodrigues, "On the Numerical Solution of Partial Differential Equations with Two Spatial Scales," *Comput. Chem. Eng.*, **21**(4), 387 (1997c).

Myers, A., "Theories of Adsorption in Micropores," *Adsorption: Science and Technology*, A. E. Rodrigues, M. D. LeVan, and D. Tondeur, eds., Kluwer, Dordrecht, The Netherlands, p. 15 (1989).

Myers, A., and J. M. Prausnitz, "Thermodynamics of Mixed-Gas Adsorption," *AIChE J.*, **11**, 121 (1965).

Ozawa, S., S. Kusumi, and Y. Ogino, "Physical Adsorption of Gases at High Pressure (IV)," *J. Colloid Interf. Sci.*, **56**, 83 (1976).

Parkyns, N. D., and D. F. Quinn, "Natural Gas Adsorbed on Carbon," *Porosity in Carbons*, J. W. Patrick, ed., chap. 11, Arnold, London, p. 291 (1995).

Pedersen, A. S., and B. Larsen, "Adsorption of Methane and Natural Gas on Six Carbons," Rep. Risø-M-2781, Risø National Laboratory, Denmark (1989).

Reich, R., W. T. Ziegler, and K. A. Rogers, "Adsorption of Methane, Ethane, and Ethylene Gases and Their Binary and Ternary Mixtures and Carbon Dioxide on Activated Carbon at 212–301 K and Pressures to 35 Atmospheres," *Ind. Eng. Chem. Process Des. Dev.*, **19**, 336 (1980).

Reid, R. C., J. M. Prausnitz, and T. K. Sherwood, *The Properties of Gases and Liquids*, 3rd ed., McGraw-Hill, New York (1977).

Remick, R. J., R. H. Elkins, E. H. Camara, and T. Bulicz, "Advanced Onboard Storage Concepts for Natural Gas-Fueled Automotive Vehicles," Rep. DOE/NASA/0327-1 prepared for U.S. Dept. of Energy and NASA, Washington, DC (1984).

Remick, R. J., and A. J. Tiller, "Heat Generation in Natural Gas Adsorption Systems," Gaseous Fuels for Transportation Int. Conf., Vancouver, B.C., Canada (1986).

Sangani, N., "Desorption Dynamics of Adsorptive Gas Storage Systems," MS Thesis, Dept. of Chemical Engineering, Cleveland State Univ., Cleveland, OH (1990).

Sejnoha, M., R. Chahine, W. Yaïci, and T. K. Bose, "Adsorption Storage of Natural Gas on Activated Carbon," AIChE Meeting, San Francisco, CA (1994).

Stoeckli, F., *Porosity in Carbons*, J. Patrick, ed., Arnold, London, p. 67 (1995).

Stoeckli, F., D. Wintgens, A. Lavanchy, and M. Stöckli, "Binary Adsorption of Vapours in Active Carbons Described by the Combined Theories of Myers-Prausnitz and Dubinin (II)," *Adsorp. Sci. Technol.*, **15**, 677 (1997).

Strisna, F., W. E. BeVier, R. Coleman, and S. Gauthier, "Adsorbent Storage of Natural Gas," *Proc. Windsor Workshop on Alternative Fuels*, p. 58 (1989).

Talu, O., "An Overview of Adsorptive Storage of Natural Gas," *Proc. Int. Conf. on Fundamentals of Adsorption*, M. Suzuki, ed., Kyoto, Japan, p. 655 (1992).

Talu, O., "Use of Additives to Increase Adsorptive Storage Capacity," *Proc. First Separations Division Topical Conf. on Separations Technologies: New Developments and Opportunities*, AIChE, Miami Beach, FL, p. 409 (1993).

Wilke, C. R., *Chem. Eng. Prog.*, **46**, 95 (1950).

Yang, R. T., *Gas Separation by Adsorption Processes*, Butterworth, Boston (1987).

Manuscript received Jan. 4, 1999, and revision received Feb. 24, 1999.